Supplementary Information

Magnetic soft millirobot with simultaneous locomotion and sensing capability

Weihong Zeng[1, #], Xinrui Ding[2, #], Yuan Jin[3, #], Bin Liu[4], Runhao Zeng[5,*], Feng Gong[1], Yan Lou[1], Lelun Jiang[4,*], Hui Li[1, *]

1. Guangdong Provincial Key Laboratory of Micro/Nano Optomechatronics Engineering, College of Mechatronics and Control Engineering, Shenzhen University, Shenzhen 518060, China
2. School of Mechanical and Automotive Engineering, South China University of Technology, Guangzhou 510640, China
3. School of Mechanical Engineering and Mechanics, Ningbo University, Ningbo 315211, China
4. School of Biomedical Engineering, Shenzhen Campus of Sun Yat-sen University, Shenzhen 518107, China
5. Artificial Intelligence Research Institute, Shenzhen MSU-BIT University, Shenzhen, 518172, China

Corresponding authors

Email addresses: zengrh@smbu.edu.cn (R. Zeng), jianglel@mail.sysu.edu.cn (L. Jiang) , huili@szu.edu.cn (H. Li)

This “Supplementary Information” includes:

Supplementary Note 1

Supplementary Figure 1–24

Supplementary Table 1–2

Supplementary Movie 1–7

Supplementary Note 1

Numerical Modeling of jet printing process.

The computation model of jet printing was constructed with idealizations based on the following assumptions:

(1) Due to the axisymmetric nature of the flow field and geometric setup of the system, a two-dimensional axisymmetric model is utilized to improve the accuracy and efficiency of the simulation.

(2) The influence of the wettability on the internal surface was not taken into consideration.

(3) Time requirement for the falling droplet to reach the steady state is long, so the we merely computed and analyze the results in partial time.

According to the assumptions above, the continuity and momentum conservation equations for the printing head section are as follows.

The continuity equation:

$$\frac{\partial \rho}{\partial t} + \nabla \cdot (\rho \boldsymbol{u}) = 0 \tag{1}$$

The momentum equation:

$$\frac{\partial (\rho u)}{\partial t} + \nabla \cdot (\rho u \boldsymbol{u}) = -\nabla p + \nabla \cdot (\mu \nabla u) + \boldsymbol{F_s} \tag{2}$$

where ρ is the density (kg/m^3), $\boldsymbol{u}$ is the velocity vector (m/s), μ is dynamic viscosity of the fluid (mPa·s), and p is the hydrostatic pressure (Pa). $\boldsymbol{F_s}$ is the surface tension force.

The surface tension force is calculated by the continuum body surface model, and a volume equivalent surface tension force is used as,

$$\boldsymbol{F_s} = \sigma \kappa \nabla A$$

where σ is the surface tension coefficient, κ is the curvature of the surface, and A is the unit surface normal vector.

In order to track the movement of the liquid-gas interface, Level Set Method (LSM) was employed. A thin layer was used to represent the liquid-gas interface, where the physical properties vary from the gas phase to the liquid phase. The model were presented by the following equations [1],

$$\rho = \rho_g + (\rho_l - \rho_g)\phi$$

$$\mu = \mu_g + (\mu_l - \mu_g)\phi$$

Subscript l and g represent the liquid and the gas phase, respectively.

For the reason that the fluid flow was mainly caused by the displacement of the needle, dynamic mesh was applied, where spring-based smoothing method and local remeshing method was used together. The triangle mesh was refined until the droplet diameter on the substrate differed by less than 0.1 μm when compared with a finer mesh. The aforementioned governing equations and boundary conditions are discretized, and the results of the discretization are solved with pressure-based solver and SIMPLE algorithm.

Supplementary Figure

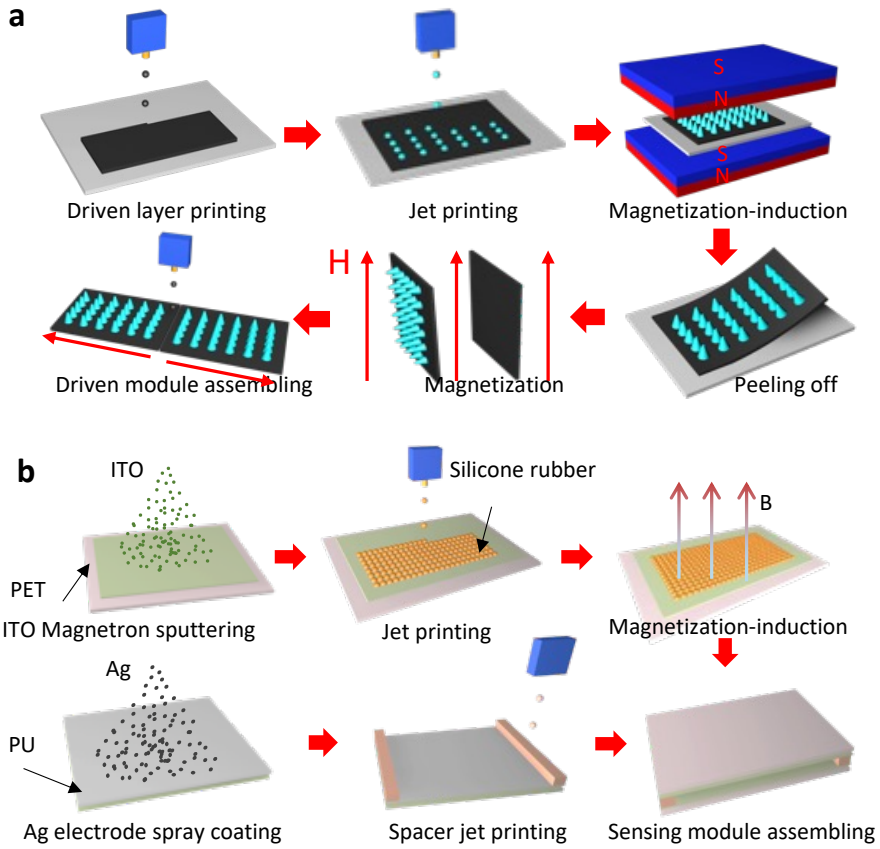

Supplementary Fig.1 Fabrication of magnetic soft millirobot. a. Fabrication process of the driven module. **b.** Fabrication process of the sensing module.

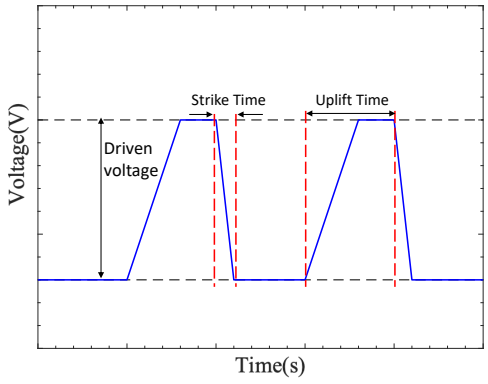

Supplementary Fig.2 Voltage parameters of piezoelectric-pneumatic material jet printing system

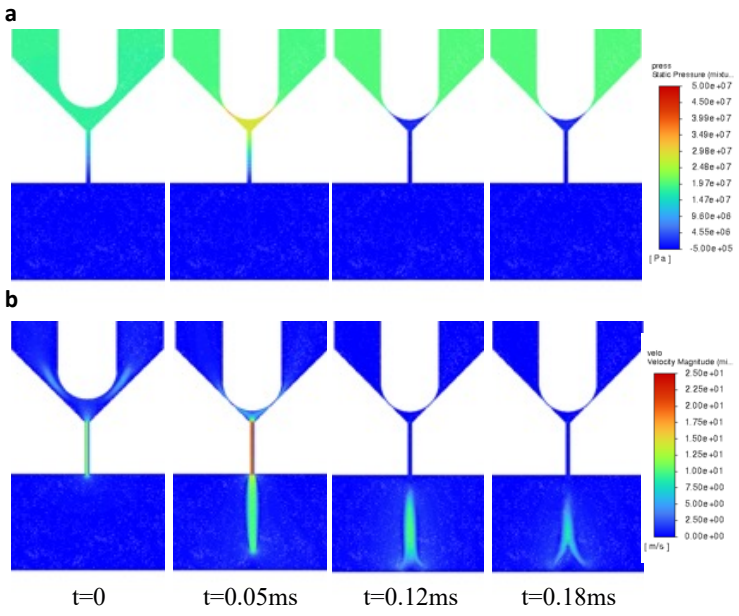

Supplementary Fig.3 Fluid velocity and pressure distribution during jet printing. a. Pressure distribution. **b.** Velocity distribution.

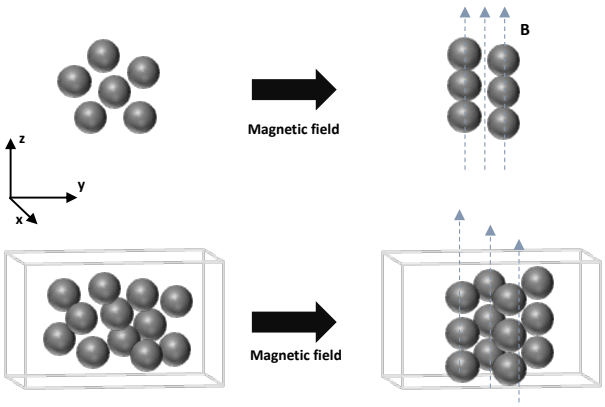

Supplementary Fig.4 Generation mechanism for the microconical matrix. When the magnetic fluid is applied, the adjacent powders would form aligned chains due to the magnetic interaction and aggregate into networks to drive the viscous fluid to grow upwards.

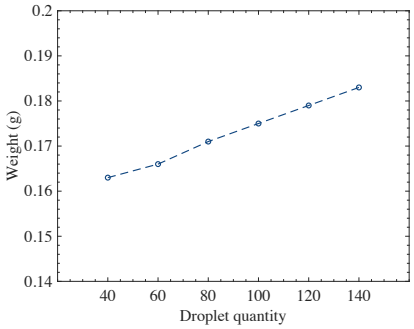

Supplementary Fig.5 Weight of the microconical matrix. When the quantity increases, the weight of millirobot also rises.

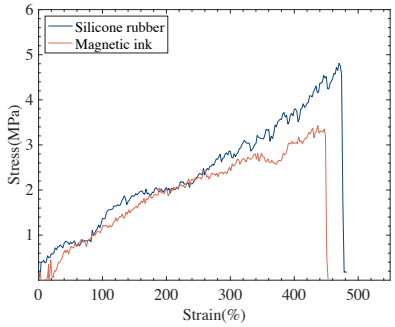

Supplementary Fig.6 Uniaxial tensile test of magnetic ink.

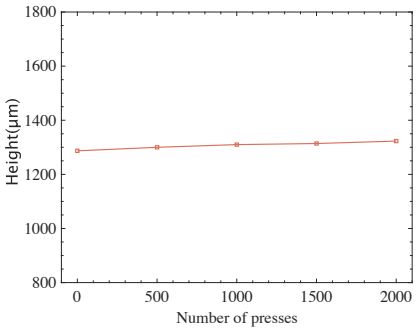

Supplementary Fig.7 Durability of the multi-legged microconical matrix

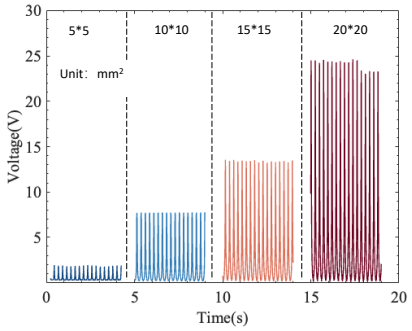

Supplementary Fig.8 Effect of electrode size on output voltage

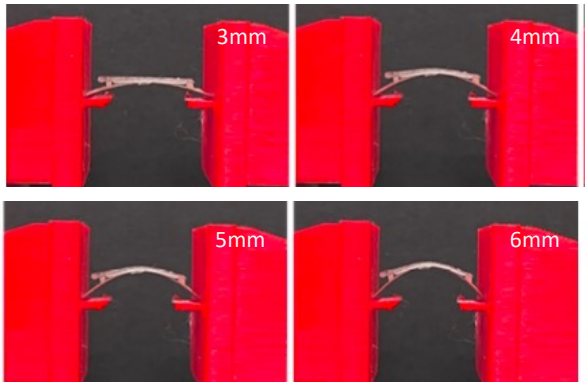

Supplementary Fig.9 Optical images for effect of offset distance

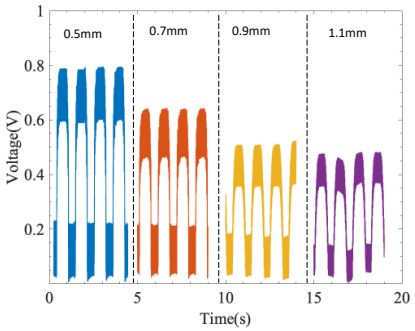

Supplementary Fig.10 Effect of droplet space for output performance in bending deformation

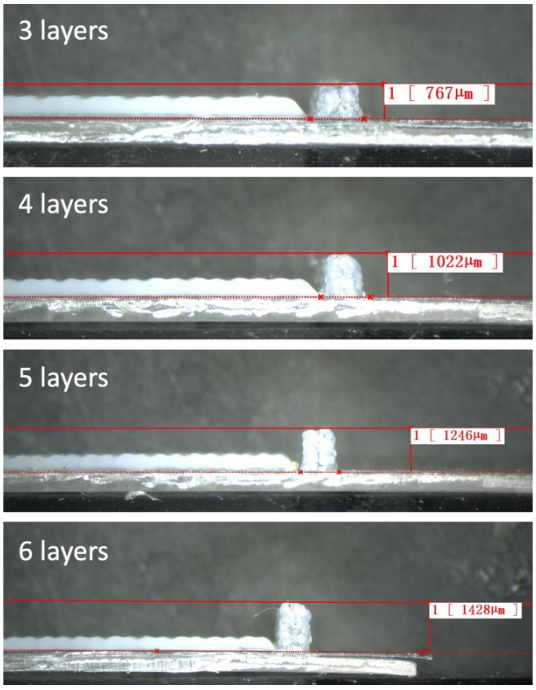

Supplementary Fig.11 Optical images for spaces inside sensing module

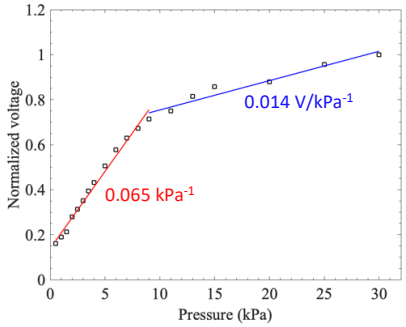

Supplementary Fig.12 Sensitivity (S) of the sensor under contact-separation mode

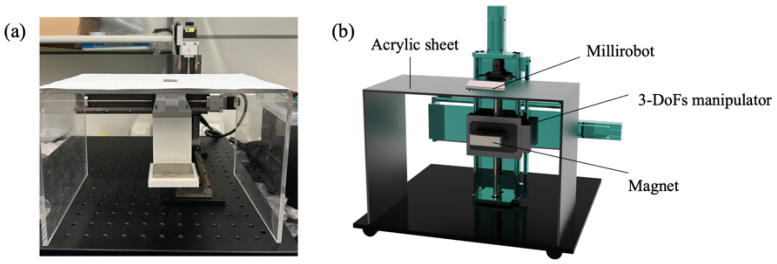

Supplementary Fig.13 Experimental setup for millirobot locomotion control

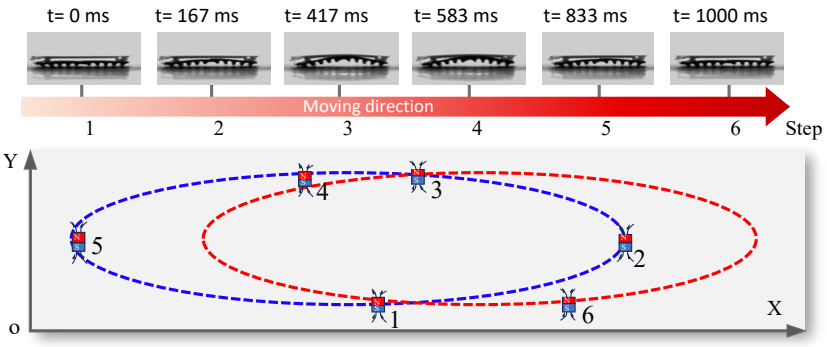

Supplementary Fig.14 Locomotion mode of millirobot under the application of an "O" shape magnetic field in the "X–Y" plane. Robot moves forward step by step with legs touching the ground.

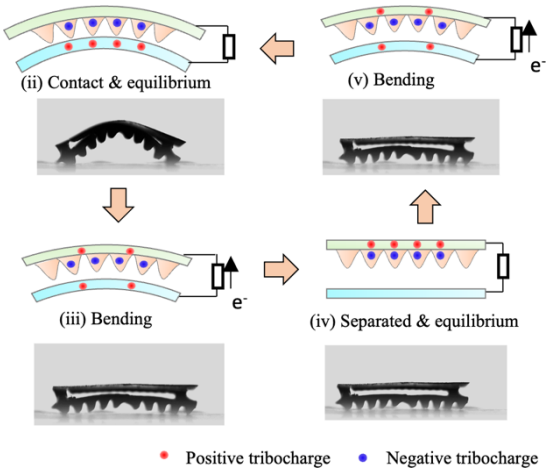

Supplementary Fig.15 Schematic diagram of the corresponding signals generated through sensing module in millirobot locomotion

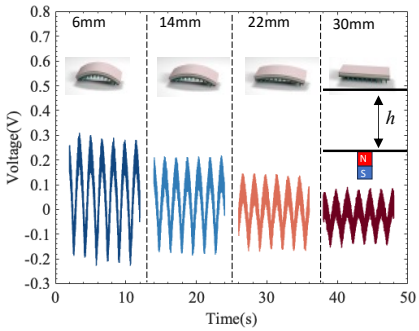

Supplementary Fig.16 Effect of permanent magnet movement in vertical direction with different distance beneath the millirobot

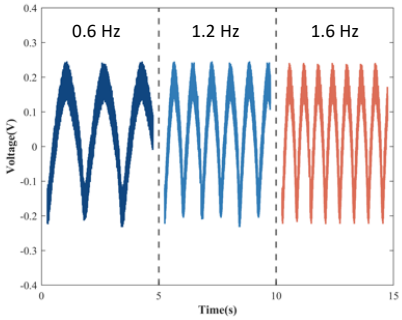

Supplementary Fig.17 Effect of permanent magnet movement frequency in vertical direction

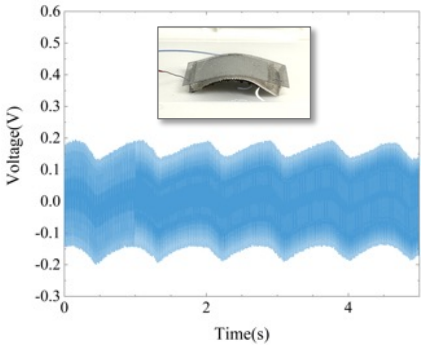

Supplementary Fig.18 Output voltages as millirobot moving in swallow water environment

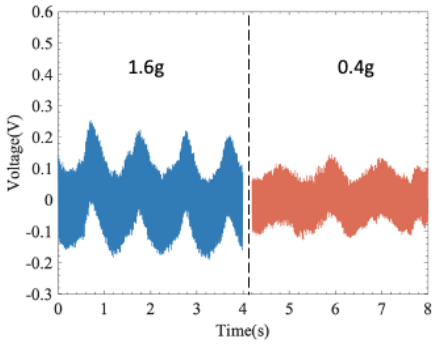

Supplementary Fig.19 Output voltages as millirobot moving with various load weights

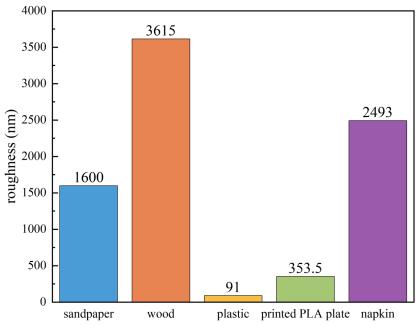

Supplementary Fig.20 Surface roughness of five terrain

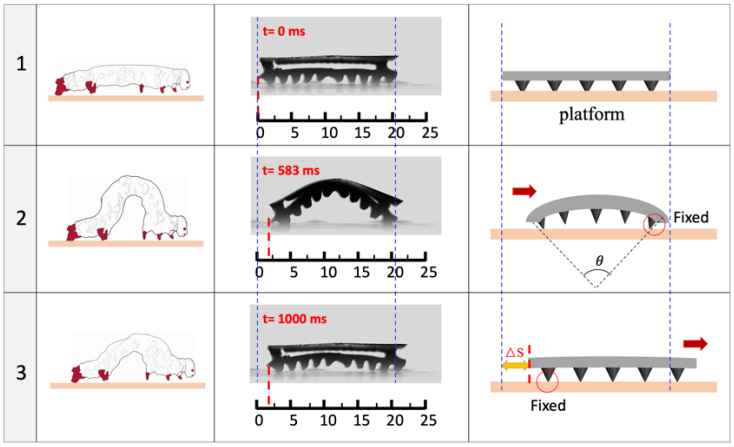

Supplementary Fig.21 Moving posture diagram of inchworm and millirobot during a crawling cycle

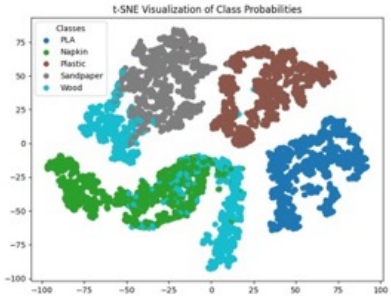

Supplementary Fig.22 T-SNE scatterplot for feature classification.

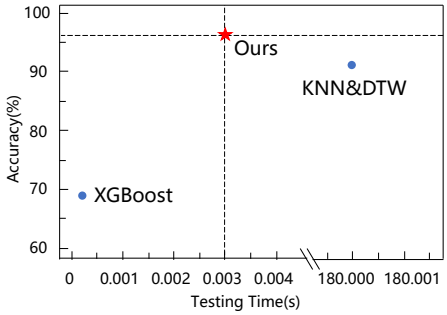

Supplementary Fig.23 Comparison of the machine learning method among ours, traditional KNN&DTW and XGBoost.

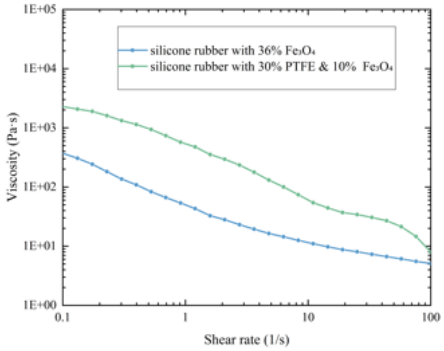

Supplementary Fig.24 Ink viscosities for Legs in driven module and sensing module

Table 1 Comparison of typical magnetic soft robot in previous studies

No.	Actuation	Fabrication method	Body mass (g)	Speed (mm/s)	Integrated sensing ability	Machine Learning application	Reference
1	Magnetic	Template modeling	0.3	22	No	No	[2]
2	Magnetic	Spin coating	0.07	2.5	No	No	[3]
3	Magnetic	Template modeling	2	0.8	No	No	[4]
4	Magnetic	3D printning	-	-	No	No	[5]
5	Magnetic	CJM	0.31	1.4	Yes	Yes	This work

Table 2 Fabrication parameters of the magnetic soft millirobot

Parameters		**Legs in driven module**	**Sensing module**
Inks	Composition/ wt%	Fe_3O_4: 36% Silicone rubber: 64%	Fe_3O_4:: 10% PTFE: 30% Silicone rubber: 60%
Jet printing	Droplet quantity	60	20

	Array	5*5	15*29
	Spacing	14 μm	0.5 μm
	Driving voltage	85 V	100 V
	Nozzle diameter	100 μm	60 μm
	printing pressure	200 MPa	200 MPa
Curing process	Curing temperature	80 ℃	60 ℃
	Curing time	10 minutes	5 minutes

Supplementary Movie 1

Jet printing process

Supplementary Movie 2

Generation process of the printed microconical matrix into legs

Supplementary Movie 3

Locomotion for soft millirobot

Supplementary Movie 4

Continuous bidirectional crawling locomotion in confined space

Supplementary Movie 5

Electric output can be acquired via the sensing module continuously

Supplementary Movie 6

Loading capacity

Supplementary Movie 7

Locomotion in various terrains

Supplementary References

1. Jiang L, Yu L, Premaratne P, Zhang Z, Qin H. CFD-based numerical modeling to predict the dimensions of printed droplets in electrohydrodynamic inkjet printing. *Journal of Manufacturing Processes* **66**, 125-132 (2021).

2. Ju Y*, et al.* Reconfigurable magnetic soft robots with multimodal locomotion. *Nano Energy* **87**, 106169 (2021).

3. Ijaz S*, et al.* Magnetically actuated miniature walking soft robot based on chained magnetic microparticles-embedded elastomer. *Sensors and Actuators A: Physical* **301**, 111707 (2020).

4. Xu R, Xu Q. Design of a bio-inspired untethered soft octopodal robot driven by magnetic field. *Biomimetics* **8**, 269 (2023).

5. Zhang Y*, et al.* Coaxially printed magnetic mechanical electrical hybrid structures with actuation and sensing functionalities. *Nature communications* **14**, 4428 (2023).